Functional and molecular profiling of hematopoietic stem cells during regeneration

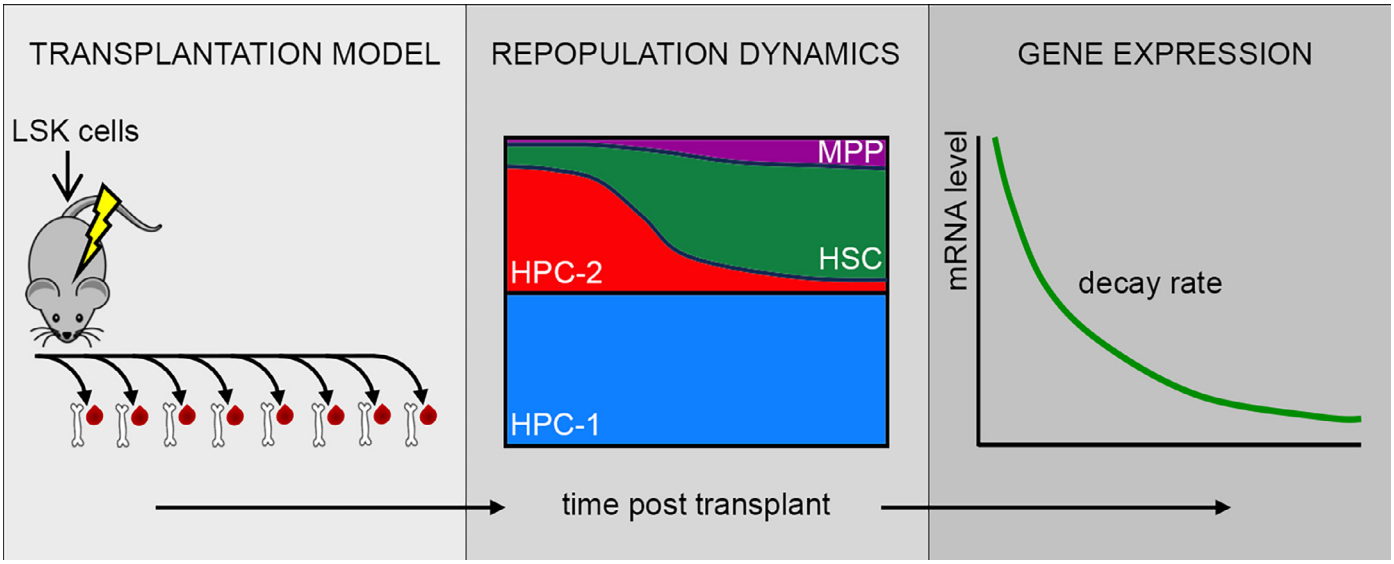

ARTICLE

Functional and molecular profiling of hematopoietic stem cells during regeneration

Anna Rydström[a], Tan H.M. Grahn[a], Abhishek Niroula[b], Els Mansell[a,1], Mark van der Garde[a,2], Maroulio Pertesi[b], Agatheeswaran Subramaniam[a], Shamit Soneji[c], Roman Zubarev[d], Tariq Enver[e,*], Björn Nilsson[b,*], Kenichi Miharada[a,3,*], Jonas Larsson[a,*], and Stefan Karlsson[a,*4]

[a]*Molecular Medicine and Gene Therapy, Lund Stem Cell Center, Lund University, Lund, Sweden;* [b]*Hematology and Transfusion Medicine, Department of Laboratory Medicine, Lund University, Lund, Sweden;* [c]*Division of Molecular Hematology, Department of Laboratory Medicine, Lund Stem Cell Center, Lund University, Lund, Sweden;* [d]*Department of Medical Biochemistry and Biophysics, Karolinska Institute, Solna, Sweden;* [e]*Stem Cell Group, Cancer Institute, University College London, United Kingdom*

Hematopoietic stem cells (HSCs) enable hematopoietic stem cell transplantation (HCT) through their ability to replenish the entire blood system. Proliferation of HSCs is linked to decreased reconstitution potential, and a precise regulation of actively dividing HSCs is thus essential to ensure long-term functionality. This regulation becomes important in the transplantation setting where HSCs undergo proliferation followed by a gradual transition to quiescence and homeostasis. Although mouse HSCs have been well studied under homeostatic conditions, the mechanisms regulating HSC activation under stress remain unclear. Here, we analyzed the different phases of regeneration after transplantation. We isolated bone marrow from mice at 8 time points after transplantation and examined the reconstitution dynamics and transcriptional profiles of stem and progenitor populations. We found that regenerating HSCs initially produced rapidly expanding progenitors and displayed distinct changes in fatty acid metabolism and glycolysis. Moreover, we observed molecular changes in cell cycle, MYC and mTOR signaling in both HSCs, and progenitor subsets. We used a decay rate model to fit the temporal transcription profiles of regenerating HSCs and identified genes with progressively decreased or increased expression after transplantation. These genes overlapped to a large extent with published gene sets associated with key aspects of HSC function, demonstrating the potential of this data set as a resource for identification of novel HSC regulators. Taken together, our study provides a detailed functional and molecular characterization of HSCs at different phases of regeneration and identifies a gene set associated with the transition from proliferation to quiescence. © 2023 ISEH – Society for Hematology and Stem Cells. Published by Elsevier Inc. This is an open access article under the CC BY license (http://creativecommons.org/licenses/by/4.0/)

HIGHLIGHTS

- Detailed map of repopulation dynamics and gene expression changes in HSPCs after transplantation.
- Early regenerating HSCs primarily produce megakaryocyte/erythroid progenitors.
- HSC reconstitution potential increases with time after transplantation.
- A decay rate model identifies genes with progressively altered expression during regeneration.

Hematopoietic stem cells (HSCs) support lifelong production of mature blood cells and need to be precisely regulated to ensure a balance between mature cellular output and long-term sustainability. Although HSCs are the only hematopoietic cells that harbor both self-renewal and long-term multilineage capacity, they do not constitute a homogenous population. Subtle differences in lineage priming and reconstitution potential create a continuum of nondiscrete HSC subtypes [1–4]. Similarly, the differentiation of HSCs into more restricted progenitors is a gradual, rather than a stepwise, process [5,6].

Advances in barcoding and single-cell sequencing have revealed differences between steady-state (SS) and perturbed hematopoiesis. In the former, long-lived progenitors, rather than HSCs, are the major contributors to native hematopoiesis [7,8]. The entire hematopoietic system is altered when exposed to severe stressors, such as transplantation or chemotherapy. For technical reasons, the dynamics of regenerative hematopoiesis is often measured in peripheral blood, where a burst of myeloid cells can initially be observed, followed by a gradual increase in the lymphoid compartment [9,10]. In the bone marrow,

*TE, BN, KM, JL, and SK contributed equally to this work.

[1]Erasmus MC Hematology, Rotterdam, The Netherlands
[2]Department of Medicine III, Hematology and Oncology, Technical University of Munich, Munich, Germany
[3]International Research Center for Medical Sciences, Kumamoto University, Kumamoto, Japan
Address correspondence to: Stefan Karlsson, Molecular Medicine and Gene Therapy, Lund Stem Cell Center, Lund University, BMC A12, 221 84 Lund, Sweden; E-mail: stefan.karlsson@med.lu.se

0301-472X/© 2023 ISEH – Society for Hematology and Stem Cells. Published by Elsevier Inc. This is an open access article under the CC BY license (http://creativecommons.org/licenses/by/4.0/)

https://doi.org/10.1016/j.exphem.2023.08.010

HSCs undergo several molecular and phenotypical changes upon regeneration. The normally quiescent and rarely cycling HSCs start proliferating to replenish the mature blood cells [11–13]. These activated HSCs alter their metabolism from glycolysis to oxidative phosphorylation and change their surface expression of several adhesion molecules that regulate interactions with the bone marrow niche [11,13,14]. Although little is known about how stress hematopoiesis influences hematopoietic progenitor populations, multipotent progenitors (MPPs) upregulate proliferation signatures, stress-response genes, and oxidative phosphorylation, suggesting that there are common molecular features between regenerating HSCs and downstream progenitors [15].

The regenerative process must be tightly regulated during acute hematopoiesis to balance the need for mature blood production while minimizing the risk of permanent stress-induced insults. Previous studies on HSC regeneration have focused on the first 1 to 3 weeks after transplantation [13,15], while the later phases of regeneration and recovery remain largely unresolved. Moreover, much effort has been centered around characterizing HSCs, while the population dynamics and molecular regulation of progenitor populations are poorly understood.

In the present study, we created an experimental situation to monitor all phases of regeneration, from the onset of activation to the return to quiescence, to better understand the population dynamics and molecular regulation of HSCs and progenitors. We hypothesized that a gradual change in stem cell functionality occurs concomitant with gradual increases or decreases in key regulatory genes. We aimed to molecularly define the regenerating hematopoietic stem and progenitor cell (HSPC) pool and identify possible novel regulators of HSCs using mathematical decay rate models.

METHODS

Mice

All experiments were approved by the Lund University Animal Ethical Committee (permit 8042/2020). Ly5.1 (B6SJL) mice were obtained from in-house breeding. Ly5.2 (C57BL/6N) mice were obtained from Janvier or Taconic. The animals were housed in ventilated racks, given autoclaved food and water, and maintained at the Biomedical Center, Lund University.

Peripheral Blood and Bone Marrow Preparation

Peripheral blood was retrieved from the tail vein and collected in Microvette tubes (Sarstedt). Before staining, erythrocytes were lysed with NH_4Cl (Stem Cell Technologies). Bone marrow cells were retrieved by crushing the femur, tibia, iliac, spine, and sternum with a mortar and pestle, filtering the suspension through a 40-μm cell strainer, followed by cKIT enrichment with anti-cKIT magnetic beads (Miltenyi Biotec) in combination with a magnetic separation system (MACS LS columns).

Flow Cytometry Analysis and Cell Sorting

For peripheral blood analysis, the following antibodies were used: CD45.1-PECy7, CD45.2-APC, GR1-FITC, CD11B-FITC, B220-FITC, B220-PECy5, and CD3e-PECy5. Cells were analyzed using Fortessa (BD). cKIT-enriched bone marrow cells were stained using the following antibodies: GR1-PECy5, CD11B-PECy5, TER119-PECy5, B220-PECy5, CD3e-PECy5, cKIT-APCe780, SCA1-BV421, CD48-FITC, CD150-PECy7, CD45.1-PE, and CD45.2-APC. Dead cells were excluded using 7-amino-actinomycin-D (7AAD). Within the Lin^-, $cKIT^+$, $SCA1^+$ population, donor ($CD45.1^+$) HPC-1 were defined as $CD48^+/CD150^-$, HPC-2 were defined as $CD48^+/CD150^+$, HSCs were defined as $CD48^-/CD150^+$, and MPPs were defined as $CD48^-/CD150^-$. Cells were sorted using FACS Aria II and Aria III (BD).

Transplantation

Recipient C57BL/6N mice were lethally irradiated with 900 cGy using a cesium source 10 hours prior to transplantation. Two hundred sorted Ly5.1 HSCs or 200–1,700 Ly5.1 HPC-2 cells were injected intravenously together with 2×10^5 whole bone marrow from Ly5.2 as support. Recipient mice were given ciprofloxacin in drinking water for 7 days after transplantation.

RNA Sequencing and Analysis

HPC-1, HPC-2, and HSCs were sorted into 10-μl phosphate-buffered saline (PBS) + RNAse inhibitor and frozen immediately at −80° C. One thousand cells were sorted for most of the samples, except for late and SS HPC-2 and early HSC samples, where cell numbers were limited (see Supplementary Table E1 for details). Complementary DNA (cDNA) synthesis and amplification were performed using SMART-Seq v4 (Takara) and AMPure XP (Beckman Coulter) according to manufacturers' instructions. For concentration measurements and size quality controls, Qubit dsDNA HS (Thermo Fisher) and Bioanalyzer High Sensitivity DNA analysis (Agilent) were used. Library preparation was performed using Nextera XT DNA library prep kit (Illumina) according to the manufacturer's instructions. Sequencing was performed using NextSeq 500 High output v2 (Illumina). Variably expressed genes were identified by calculating the variance from a fitted means using DESeq2 normalized data (http://pklab.med.harvard.edu/scw2014/subpop_tutorial.html). Hierarchical clustering was performed using the hclust function in R (https://cran.r-project.org/) using the correlation distance 1-r to define the similarity between samples. Differentially expressed genes were identified using the R package DESeq2 [16] with adjusted $p < 0.1$ and log2 fold change (FC) > 1 as thresholds after removing potential batch effects determined by using the RemoveBatchEffect function from the *limma* package [17]. Heat maps display relative expression levels for each gene and were created using Morpheus, https://software.broadinstitute.org/morpheus. Gene set enrichment analysis (GSEA) was performed using the GSEA software tool from Broad Institute [18]. Gene ontology (GO) analysis was performed by computing the overlap with other gene sets using the MSigDB tool from Broad Institute. Venn diagrams were created using Venny 2.1 (https://bioinfogp.cnb.csic.es/tools/venny/index.html). Overlap in gene expression between 2 gene sets was calculated as described below in combination with normal approximation probability:

$$RF = x/([n \times D]/N),$$

where x = number of genes in common between groups n = number of genes in group 1

D = number of genes in group 2

N = number of total genes, in this case 25,000 (estimate of protein-coding genes)

To model the temporal transcriptomic profiles of regenerating HSCs, we fitted the gene expression over time to the following equation.

$$X_t = X_0 + K\, e^{-\lambda t} \quad (1)$$

where, t is the time between 3 weeks and 16 weeks, X_t is the gene expression at time t, X_0 is the baseline gene expression, K is the scale factor, and λ is the decay rate. The transcriptomic measurements (read counts normalized by using variance stabilizing transformation) at 8 time points (3, 4, 5, 6, 8, 10, 12, and 16 weeks after transplantation) were fitted into the model. In the above equation, baseline gene expression, scale factor, and decay rate are unknown. To find the optimal scale factor and decay rate for each gene, we performed a grid search by testing all combinations of scale factor and decay rate ranging arbitrarily between −50 and 50. We performed the grid search for up to 10 iterations to find better combinations by avoiding local minima. If the minima were found at the upper or lower limits of the grid search, the limits were extended. For each combination of scale factor and decay rate, we computed the baseline expression using equation 2, and the optimal model fit was defined by the lowest value in equation 3.

$$X_0 = X_t - K\, e^{-\lambda t} \quad (2)$$

$$\left(X_t - X_0 - K\, e^{-\lambda t}\right)^2 = 0 \quad (3)$$

After identifying the optimal model, we calculated the area under the curve (AUC) of the fitted line using equation 4.

$$AUC = \int_3^{16} X_t\, d_t$$

$$AUC = \frac{K}{\lambda}\left(e^{-\lambda \times 3} - e^{-\lambda \times 16}\right) \quad (4)$$

To compute *p* values, the model was fit 1,000 times by randomly shuffling all gene expression measurements for the gene across all time points. The *p* values were computed by comparing the AUC with the distribution of the shuffled AUC using a two-tailed hypothesis test. Because random shuffling was only repeated 1,000 times for more than 10,000 genes, the *p* values were used to rank the genes fitting the model.

The RNA sequencing data were deposited in the Gene Expression Omnibus (GEO) database (Accession: GSE241088).

Quantitative Polymerase Chain Reaction

Five hundred HSCs were sorted into 8 μl of lysis buffer (0.4% NP-40, 65-μM deoxynucleotide tri-phosphate (dNTP), 2.3-mM dithiothreitol (DTT), and 1.2-mM RNAseOUT (ThermoFisher)). cDNA synthesis followed by 10 cycles of targeted preamplification was performed using CellsDirect kit (Invitrogen, #11753100) and pooled gene-specific TaqMan probes (*Itm2a*: Mm00515208_m1, *Nrxn1*: Mm00660298_m1, *Plscr4*: Mm00618662_m1, *Rap1b*: Mm05911819_s1, *Srm*: Mm00726089_s1, *Gp9*: Mm00497671_g1, *Tmem40*: Mm00460636_m1, *Phb2*: Mm00476104_m1, *Imp4*: Mm00618061, *Actb*: Mm01205647_g1, and *Hprt*: Mm03024075_m1) (Fisher Scientific). The following polymerase chain reaction (PCR) program was used: 50°C for 60 min, 95°C for 2 min, 10 × (95°C for 15 sec, 60°C for 4 min). One microliter of preamplified DNA was used for downstream real-time quantitative PCR (qPCR) using TaqMan gene expression master mix (Fisher Scientific, #4369016) together with the individual probes listed above on 7900HT Fast Real-Time PCR system (Applied Biosystems). Gene expression levels were normalized to the housekeeping gene *Hprt* and adjusted to 1 for the 16-week samples.

Statistical Analysis

Statistical analysis was performed using GraphPad Prism 9. Results are represented as mean ± SD or median with 95% CI, as indicated in figure legends. When comparing more than 2 groups with non-Gaussian distribution, the Kruskal-Wallis test was used with Dunn's correction for multiple comparisons. When comparing more than 2 groups with Gaussian distribution, ordinary 1-way analysis of variance (ANOVA) in combination with Tukey's or Dunnett's multiple comparisons test or Brown-Forsythe and Welch ANOVA test in combination with Dunnett T3 correction for multiple comparisons was used. Statistical significance is indicated as $*Padj \leq 0.05$, $**Padj \leq 0.01$, $***Padj \leq 0.001$, and $****Padj \leq 0.0001$, and *N* denotes the number of biological replicates.

RESULTS

Hematopoietic Repopulation Dynamics After Transplantation

To generate a model in which HSPCs could be isolated and analyzed at different phases of regeneration, we transplanted 8,000 Lin^-, $cKIT^+$, and $SCA1^+$ cells (LSK) from Ly5.1 B6SJL mice into lethally irradiated Ly5.2 C57Bl/6 recipients. The recipient mice were then euthanized for blood and bone marrow analyses at 8 different time points after transplantation (3, 4, 5, 6, 8, 10, 13, and 16 weeks) to monitor the repopulation dynamics over time. Blood and bone marrow from nontransplanted SS control mice were analyzed in the same way to serve as reference cells (Figure 1A).

Peripheral blood analysis of the recipient mice showed a high overall donor reconstitution that increased over time (Figure 1B). In line with other reports [9,10], donor lineage distribution analysis revealed a predominant myeloid production during early regeneration. At 6 weeks, the donor lineage distribution resembled that of SS mice with a larger lymphoid component (Figure 1C). In the bone marrow, the donor cells constituted more than 90% of cells at all time points analyzed (Figure 1D). We further analyzed the stem and progenitor cell SLAM subsets within the bone marrow LSK population, including HSCs (LSK, $CD48^-$, $CD150^+$), HPC-1 (LSK, $CD48^+$, $CD150^-$), HPC-2 (LSK, $CD48^+$, $CD150^+$), and MPPs (LSK, $CD48^-$, $CD150^-$) (Figure 1E, F and Supplementary Figure E1). The early regenerative phase, defined as 3−4 weeks after transplantation, was characterized by a substantial increase in the proportion of HPC-2, concomitant with reduced proportions of the MPPs and HSCs (Figure 1E, F and Supplementary Figure E1C−E). These findings suggest that the initial output from transplanted LSK cells is aimed at rapidly producing megakaryocyte (MK) and erythroid progenitors [13], rather than reconstituting the HSC pool. During the intermediate phase of regeneration, defined as 8−10 weeks after transplantation, the proportion of HPC-2 gradually decreased, whereas the proportion of MPPs and HSCs increased. During the late regeneration phase, 13−16 weeks after transplantation, the LSK subset populations displayed a similar distribution as in SS mice. The HPC-1

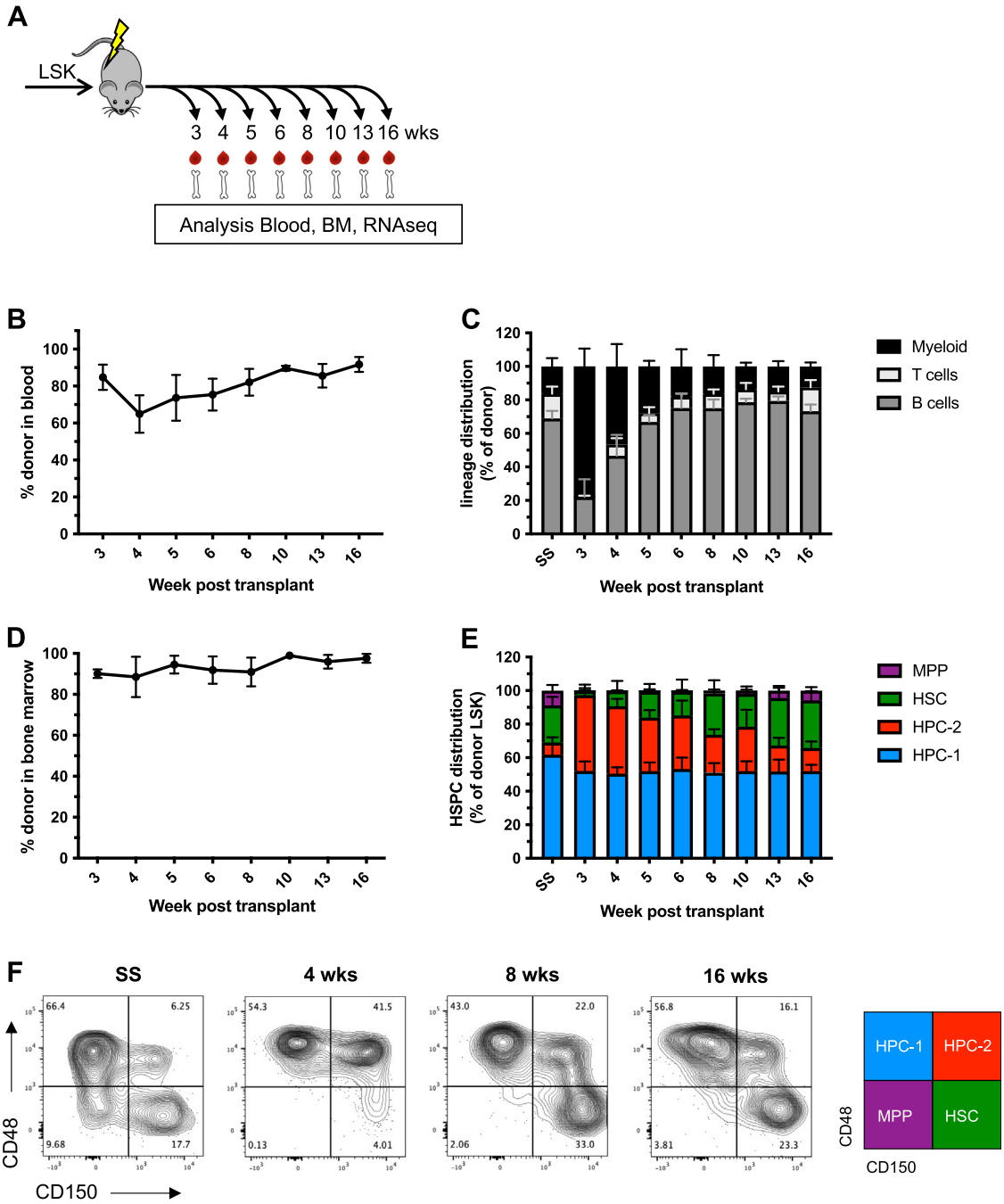

Figure 1 Reconstitution kinetics in blood and bone marrow (BM) after transplantation. **(A)** Eight thousand LSK cells from Ly5.1 donor mice were transplanted with 200,000 whole BM support from Ly5.2 mice into lethally irradiated Ly5.2 recipients. The recipients were euthanized for phenotypic blood and BM analyses and RNA sequencing (RNAseq) of sorted HPC-1, HPC-2, and HSCs, 3, 4, 5, 6, 8, 10, 13, and 16 weeks after transplantation.

(B) Ly5.1 donor chimerism in the blood of primary transplanted recipients. **(C)** Lineage distribution of Ly5.1 donor B, T, and myeloid (M) cells in the blood of primary transplanted recipients. **(D)** Ly5.1 donor chimerism in the BM of primary transplanted recipients.

(E) Distribution of HPC-1, HPC-2, HSC, and MPP within donor LSK in the BM of primary transplanted recipients. **(F)** Representative flow cytometry plots of HPC-1, HPC-2, HSC, and MPP from steady-state BM and BM isolated from primary recipients 4, 8, and 16 weeks after transplantation. All data represent mean ± SD. N = 3 to 17 mice per condition from 2 separate experiments.

population, which contains both myeloid and lymphoid progenitors, did not exhibit any major relative or absolute changes during the 16 weeks observed (Figure 1E, F and Supplementary Figure E1B).

In conclusion, hematopoietic regeneration after transplantation is initially dominated by the production of myeloid cells, in both blood and bone marrow. In particular, the HPC-2 population initially expanded, whereas the primitive MPP and HSC populations displayed a delayed recovery. Additionally, the peripheral blood composition reaches SS equilibrium with faster kinetics compared to the stem and progenitor populations in the bone marrow.

HSC Reconstitution Potential Increases with Time After Primary Transplantation

To functionally assess the serial reconstitution potential of primary transplanted cells from different stages of regeneration, we sorted 200 regenerating HSCs from primary recipients at 4, 8, and 16 weeks for transplantation into secondary recipients (Figure 2A). Compared to freshly isolated SS HSCs, the regenerating HSCs had significantly reduced engraftment capacity (Figure 2B, C). Although not statistically significant, there was a clear trend of increasing engraftment potential from reisolated regenerating HSCs over time after the primary transplantation, which was observed in both peripheral blood and bone marrow at 16 weeks after the serial transplantation (Figure 2B, C). This finding indicates that regenerating HSCs partially regain their reconstitution capacity over time after transplantation. Similar observations were previously reported by Pietras et al [13], although with faster kinetics and higher cell doses. The peripheral blood lineage distribution from the serially transplanted HSC groups displayed similar kinetics, with delayed B-cell recovery compared to primary transplanted SS HSCs (Figure 2D). However, at the end point, both donor peripheral blood lineage distribution and bone marrow LSK distribution were similar between all groups (Figure 2D, E).

Given the transient relative expansion of HPC-2 during the early phase, we wanted to investigate if this population contained any functional stem cells. Although the phenotypic HPC-2 population in SS mice has been shown not to contain stem cell activity [13,19], it is currently unknown whether the same holds true for the regenerating HPC-2 population. For this purpose, we isolated and transplanted 200–1,700 HPC-2 cells from mice at 4 weeks after primary transplantation, a time point when the relative HPC-2 population was at its highest. In line with the observations of the SS HPC-2 population, peripheral blood donor contribution did not reach above 1% (Figure 2B), demonstrating that the regenerating HPC-2 population does not contain stem cell activity.

Global Gene Expression Analysis Reveals Distinct Features of Regenerating HSPCs

To investigate the transcriptional changes taking place in HSPCs in response to transplantation, we performed bulk RNA sequencing on HPC-1, HPC-2, and HSC populations at 3, 4, 5, 6, 8, 10, 13, and 16 weeks after primary transplantation and on the same populations from SS mice. Owing to limiting cell numbers, the MPP population was not included. Hierarchical clustering based on the 1,000 most variable genes between all samples revealed 3 main clusters principally containing one of the HSPC subsets each, with no clear pattern associated with the time after transplantation (Supplementary Figure E2), suggesting that population identity is a stronger determinant of the global transcriptome than the effect of transplantation.

We identified several population-defining genes, including lymphoid genes (*Flt3, Notch1*, and *Rag2*) in HPC-1, myeloerythroid genes (*Gata1, Gata2*, and *Klf1*) in HPC-2, and stem cell genes (*Mpl, Hoxb5*, and *Socs2*) in HSC, to be differentially expressed between these populations (Figure 3A). Moreover, messenger RNAs (mRNA) of markers used for sorting (*CD48* and *Slamf1*) were expressed according to phenotype. Interestingly, HPC-2–defining genes were also expressed in early HSC samples, and conversely, some stem cell genes were lowly expressed in early and intermediate HPC-2, underlining the close connection between these populations [13,20–22]. In conclusion, HSPC populations maintain their molecular identity through all phases of reconstitution while at the same time undergoing gradual changes as a consequence of transplantation.

To analyze which cellular processes are induced by transplantation, we conducted GSEA between different regenerative phases within the defined HSPC populations. To this end, week 3–4 samples, week 8–10 samples, and week 13–16 samples from each population were pooled into early, intermediate, and late categories, respectively. In addition to allowing for increased sample size, this grouping is representative of the functional assessment by transplantation, as shown in Figure 2. All significantly enriched Hallmark gene sets from pairwise comparisons of early versus intermediate and early versus late samples (false discovery rate [FDR] q value < 0.05), are depicted in Figure 3B, C, respectively.

HPC-1, HPC-2, and HSCs were all enriched for cell cycle signatures (E2F targets, G2M checkpoint) in the early compared to intermediate samples, demonstrating the strong demand for the production of mature blood cells after transplantation. Moreover, early HSC and HPC-1 subsets were enriched for genes associated with Myc and mTOR signaling, which are key regulatory pathways for controlling proliferation and metabolic switches [23–26]. Genes belonging to fatty acid metabolism and glycolysis gene sets were, however, uniquely enriched in early HSCs, highlighting an important difference between HSCs and more committed progenitors [23,24,27,28], as reviewed by Oburoglu et al [29]. Similarly, genes in the peroxisome gene set were expressed more specifically in early than in intermediate HSCs, supporting previous findings by Broxmeyer et al [30] and Ito et al [27] connecting peroxisome and mitochondrial function with HSC expansion through metabolic regulation. Genes associated with heme metabolism, coagulation, and complement system were enriched in early compared to late HSCs, possibly reflecting a subpopulation of HSCs primed to differentiate toward HPC-2. Genes regulating tumor necrosis factor (TNF) signaling via nuclear factor kappa B (NFkB) were enriched in intermediate compared to early samples in all populations. Yamashita and Passegué [31] recently reported that TNF acts as a pro-survival signal specifically in HSCs, suggesting that this pathway might be important during the intermediate phase of reconstitution after transplantation. Genes associated with both interferon (IFN) α and γ responses were enriched in early compared to late HPC-1 and HPC-2 but not in HSCs. IFN signaling has been shown to induce proliferation in HSCs as well [32–34], and it is possible that at 3–4 weeks after transplantation, HSCs have already downregulated their response to IFN.

Finally, we investigated whether the differences in functional output observed among early, late, and SS HSCs were reflected in their transcriptome profile. Indeed, a comparison of early versus late HSCs with published gene sets of long-term HSC function [35,36] revealed

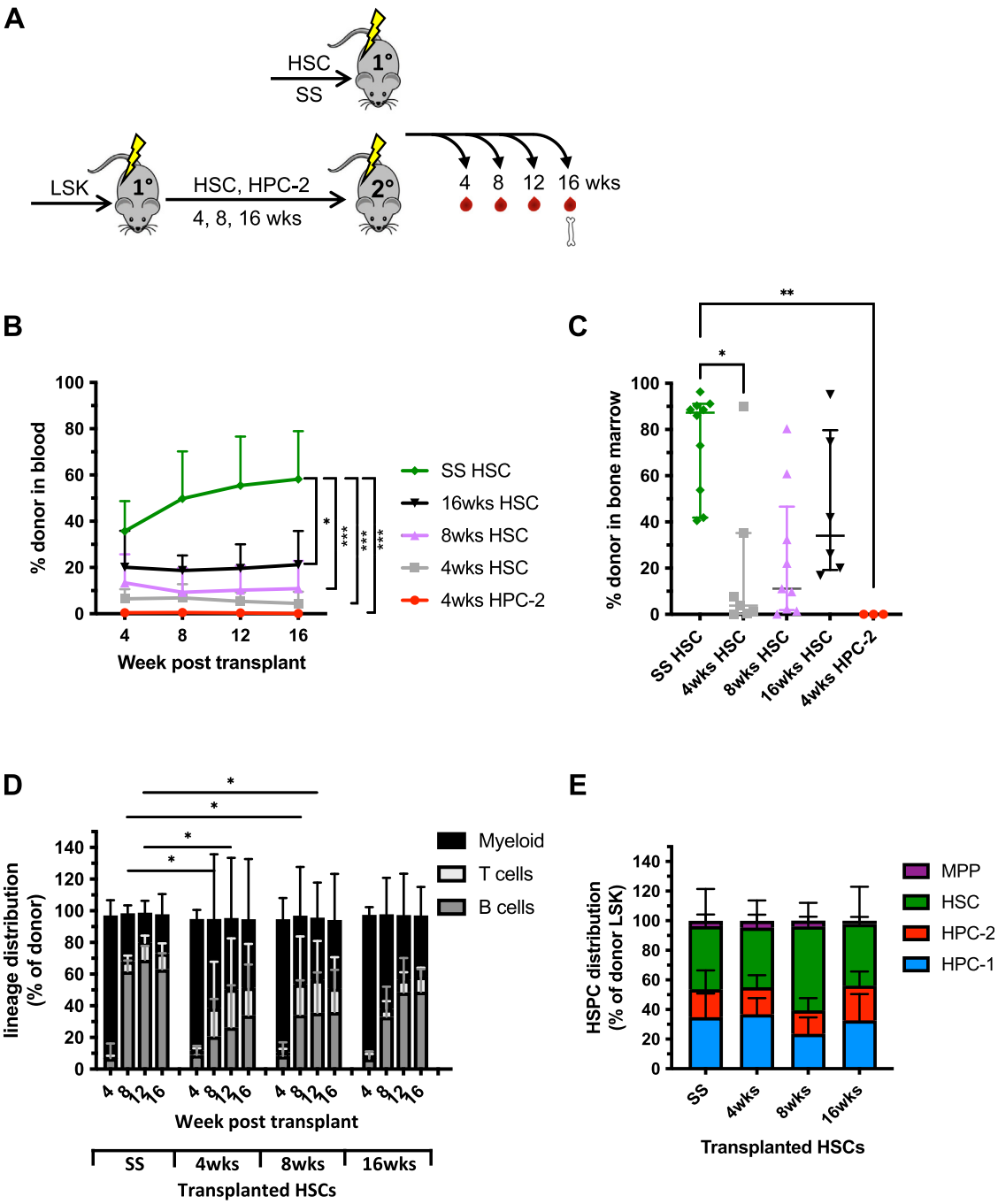

Figure 2 Reconstitution potential of regenerating HSCs and HPC-2. **(A)** Eight thousand LSK cells from Ly5.1 donor mice were transplanted with 200,000 whole bone marrow support from Ly5.2 mice into lethally irradiated Ly5.2 recipients. At 4, 8, and 16 weeks after primary transplantation 200 HSCs were sorted and retransplanted into secondary recipients. In addition, at 4 weeks after primary transplantation 200–1,700 HPC-2 cells were transplanted into secondary recipients. As a reference, 200 HSCs from SS donors were transplanted into primary recipients. **(B)** Donor chimerism in the blood of 1° recipients transplanted with 200 SS HSCs (green line), 2° recipients transplanted with 200 HSCs isolated at 4 (light gray line), 8 (magenta line), and 16 weeks (black line), and 2° recipients transplanted with 200–1,700 HPC-2 isolated at 4 weeks (red line). Data are represented as mean ± SD. N = 6–9 mice per condition from 2 separate experiments. Statistical significance was calculated using Brown-Forsythe and Welch ANOVA tests in combination with Dunnett T3 correction for multiple comparisons. Significance is indicated as *$Padj \leq 0.05$; **$Padj \leq 0.01$; ***$Padj \leq 0.001$. **(C)** Donor chimerism in the bone marrow of transplanted recipients described in **(A)**. Data represented as median with 95% CI. Statistical significance was calculated using Kruskal-Wallis test in combination with Dunn's correction for multiple comparisons. Significance is indicated as *$Padj \leq 0.05$; **$Padj \leq 0.01$. **(D)** Lineage distribution of donor cells in the blood of transplanted recipients described in **(A)**. Data represented as mean ± SD. **(E)** Distribution of HPC-1, HPC-2, HSC, and MPP within donor LSK in the bone marrow of transplanted recipients described in **(A)**. Data represented as mean ± SD.

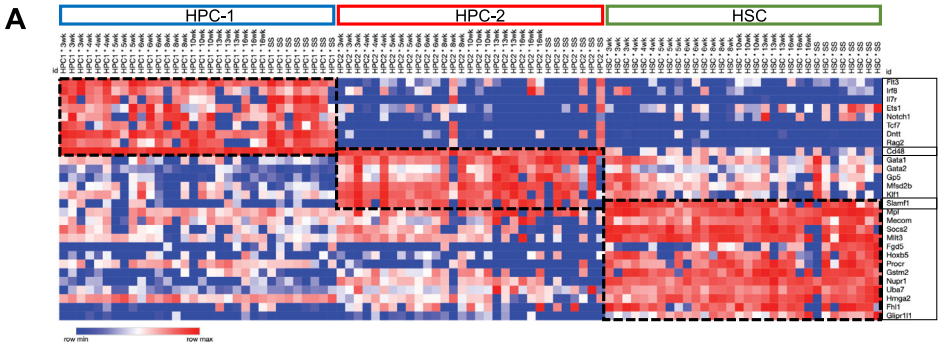

B

HPC-1 Early vs Intermediate	NES	FDR q-val
E2F_TARGETS	1.86	0.003
G2M_CHECKPOINT	1.81	0.002
MYC_TARGETS_V2	1.67	0.012
MTORC1_SIGNALING	1.56	0.036
PI3K_AKT_MTOR_SIGNALING	1.55	0.033
MYC_TARGETS_V1	1.51	0.044
TNFA_SIGNALING_VIA_NFKB	-2.7	0

HPC-2 Early vs Intermediate	NES	FDR q-val
INTERFERON_ALPHA_RESPONSE	1.9	0.001
HEME_METABOLISM	1.79	0.003
INTERFERON_GAMMA_RESPONSE	1.71	0.007
G2M_CHECKPOINT	1.62	0.021
E2F_TARGETS	1.54	0.037
TNFA_SIGNALING_VIA_NFKB	-3.04	0
HYPOXIA	-1.87	0.009
P53_PATHWAY	-1.82	0.011
EPITHELIAL_MESENCHYMAL_TRANSITION	-1.78	0.011
APOPTOSIS	-1.61	0.037

HSC Early vs Intermediate	NES	FDR q-val
E2F_TARGETS	2.44	0
MYC_TARGETS_V1	2.33	0
MTORC1_SIGNALING	2.21	0
G2M_CHECKPOINT	2.2	0
MYC_TARGETS_V2	2.03	0
FATTY_ACID_METABOLISM	1.84	1.00E-03
PI3K_AKT_MTOR_SIGNALING	1.82	1.00E-03
HEME_METABOLISM	1.71	0.005
GLYCOLYSIS	1.66	0.008
UNFOLDED_PROTEIN_RESPONSE	1.63	0.01
ADIPOGENESIS	1.61	0.011
PEROXISOME	1.58	0.014
UV_RESPONSE_UP	1.5	0.028
SPERMATOGENESIS	1.48	0.033
TNFA_SIGNALING_VIA_NFKB	-2.46	0

C

HPC-1 Early vs Late	NES	FDR q-val
INTERFERON_ALPHA_RESPONSE	1.94	0.002
INTERFERON_GAMMA_RESPONSE	1.86	0.002
ALLOGRAFT_REJECTION	1.73	0.006
WNT_BETA_CATENIN_SIGNALING	1.66	0.013
G2M_CHECKPOINT	1.62	0.018
INFLAMMATORY_RESPONSE	1.59	0.022
IL6_JAK_STAT3_SIGNALING	1.54	0.034
UV_RESPONSE_UP	1.54	0.032
PI3K_AKT_MTOR_SIGNALING	1.5	0.043

HPC2_Early vs Late	NES	FDR q-val
KRAS_SIGNALING_DN	1.87	0.008
INTERFERON_GAMMA_RESPONSE	1.75	0.016
INTERFERON_ALPHA_RESPONSE	1.71	0.016
EPITHELIAL_MESENCHYMAL_TRANSITION	1.61	0.033
INFLAMMATORY_RESPONSE	1.6	0.028
IL6_JAK_STAT3_SIGNALING	1.54	0.038
E2F_TARGETS	-2.27	0
G2M_CHECKPOINT	-1.77	0.01
FATTY_ACID_METABOLISM	-1.62	0.041

HSC Early vs Late	NES	FDR q-val
E2F_TARGETS	2.37	0
MYC_TARGETS_V1	2.22	0
MTORC1_SIGNALING	2.18	0
G2M_CHECKPOINT	2.09	0
MYC_TARGETS_V2	1.95	0
GLYCOLYSIS	1.86	0.002
UV_RESPONSE_UP	1.75	0.004
HEME_METABOLISM	1.71	0.006
UNFOLDED_PROTEIN_RESPONSE	1.67	0.007
ADIPOGENESIS	1.66	0.007
ESTROGEN_RESPONSE_LATE	1.66	0.007
FATTY_ACID_METABOLISM	1.66	0.007
PI3K_AKT_MTOR_SIGNALING	1.63	0.008
COAGULATION	1.49	0.041
SPERMATOGENESIS	1.48	0.041
COMPLEMENT	1.46	0.047

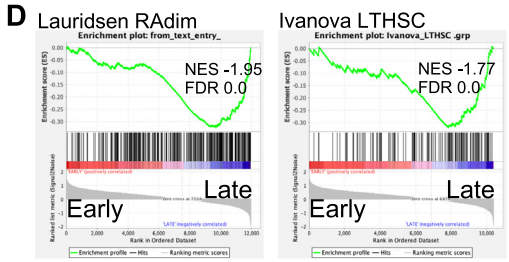

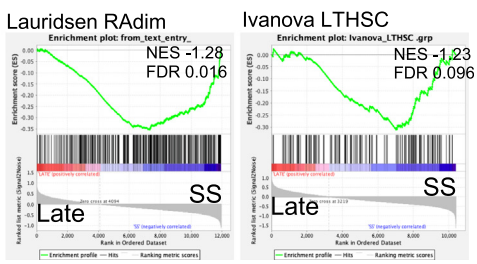

Figure 3 Global transcriptomic analysis by RNA sequencing of regenerating HPC-1, HPC-2, and HSCs. **(A)** Heat map displaying differential expression of population-defining genes in regenerating HPC-1, HPC-2, and HSC. **(B)** GSEA of early versus intermediate HPC-1, HPC-2, and HSCs against Hallmark gene sets. **(C)** GSEA of early versus late HPC-1, HPC-2, and HSC against Hallmark gene sets. **(D)** GSEA of early versus late HSCs against curated gene sets. **(E)** GSEA of Late versus SS HSCs against curated gene sets. N = 3–8. NES = normalised enrichment score. FDR = false discovery rate.

that late HSCs were enriched for genes belonging to both RAdim and LTHSC gene sets, both associated with increased stem cell fitness (Figure 3D). The difference in transcriptional states between late and SS HSCs was less pronounced. Genes belonging to the long term HSC (LTHSC) signature were not significantly enriched in either group, while the retinoic acid dim (RAdim) signature genes were enriched in SS HSCs, albeit with a lower normalized enrichment score (Figure 3E).

Integrative Analysis of Regenerating HSC Transcriptome

Within the HSC population, we found 1,060 genes to be differentially expressed between early and late samples (Figure 4A). Although we expect the largest differences to be seen between these groups, it does not capture the gradual change in HSC functionality observed in the secondary transplantations. Instead, we hypothesized that genes important in HSC regulation would successively decrease or increase their expression with time after transplantation.

To identify genes in line with this idea, we fitted the gene expression change over time to a model with a specific decay rate (λ) (Figure 4B). After fitting the RNA sequencing data of transplanted HSCs to the decay model, we prioritized 1,840 genes for further investigation ($p < 0.1$, log counts per million (CPM) > 2). In addition, we wanted to select for genes that were differentially expressed between early and SS samples ($|\log2FC| > 1$; $P\text{adj} < 0.05$, where $P\text{adj}$ is FDR adjusted p value), resulting in a final list of 130 genes (Figure 4C and Supplementary Table E2). Among the 130 genes were genes with previously described roles in HSC regulation, including *Egr1, S100a6, Pclaf, Suz12*, and *Rbbp5* [37–41]. Several genes regulating MK and erythroid differentiation (*Blvra, F2R, Gp9*, and *Fermt3)*, displayed higher expression levels in HSCs during the early phase of regneration [42–45]. GO analysis of the 117 genes with decreased expression over time confirmed the strong cell cycle signature previously observed in GSEA, as well as mitochondrial-related genes and genes involved in RNA binding (Supplementary Figure E3).

A recent study by Rodriguez-Fraticelli et al [46] identified genes differentially expressed in HSCs depending on their historical progeny output after transplantation. They correlated a MK-biased transcriptome profile with high engraftment potential in secondary recipients, while a multilineage transcriptome profile correlated with poor engraftment. When comparing our gene list to this data set and to genes differentially expressed depending on their divisional history (DH) [47], we observed a significant overlap between genes with increasing expression with time after transplantation and genes upregulated in MK-biased HSCs (representation factor, 8.5; $p < 0.001$) or downregulated with DH (representation factor, 5.5; $p < 0.001$). Conversely, genes with decreasing expression after transplantation overlapped with genes upregulated in multilineage HSCs (representation factor, 2.8; $p < 0.001$) and with DH (representation factor, 4.2; $p < 0.001$) (overlaps indicated as shaded sectors in Figure 4D, E). These significant molecular overlaps alongside our secondary transplantation data give support to a correlation between our gene list and HSC functionality.

To validate the results obtained from the RNA sequencing analysis, we isolated 500 HSCs from SS mice and at 4, 8, and 16 weeks after primary transplantation for qPCR analysis of 3 genes with increasing expression (*Itm2a, Nrxn1*, and *Plscr4*) and 6 genes with decreasing expression (*Rap1b, Srm, Gp9, Tmem40, Phb2*, and *Imp4*) after transplantation (Figure 4F and Supplementary Figure E4A). All 9 selected genes had previously unknown roles in HSC regulation but described biological processes associated with stem cell function. For example, *Plscr4* is a regulator of plasma membrane asymmetry [48]; *Itm2a*, a negative regulator of autophagy [49]; *Rap1b* is involved in the formation of hemogenic endothelium [50,51]; *Srm*, a direct target of Myc [52]. Six out of these 9 genes displayed similar expression dynamics in the RNA sequencing analysis in the qPCR analysis, corroborating the robustness of the RNA sequencing analysis (Figure 4G and Supplementary Figure E4B).

In conclusion, by fitting transcriptomes from HSCs during the entire regeneration phase to a decay rate model, we identified 130 genes with progressively decreased or increased expression after transplantation. The significant overlap with previously published gene sets linked to HSC function, in combination with qPCR validation, shows the potential of this data set.

DISCUSSION

This study aimed to molecularly characterize regenerating HSPCs after transplantation and to use a decay rate model to identify genes with altered expression in HSCs. Additionally, to understand the population kinetics, we performed a comprehensive analysis of the HSPC populations in combination with peripheral blood analysis during 16 weeks after transplantation.

Our main observation is the initial expansion of HPC-2 and a decrease in HSC and MPP, followed by a gradual decrease in HPC-2 and an increase in HSC. The increase in HPC-2 most likely reflects a response to meet the immediate demand for MK/platelet and erythrocyte production after myeloablation. Although global transcriptomic analysis showed that regenerating HPC-1, HPC-2, and HSCs maintain their population identity, we observed coexpression of population-defining genes between early-phase HPC-2 and HSC as well as higher expression of genes regulating MK and erythrocyte differentiation in early-phase HSCs, suggesting that a subpopulation of these HSCs may be primed to differentiate toward HPC-2. This aligns with previous reports identifying HPC-2 as a transient myeloid-biased progenitor population and as one of the first emerging populations from HSCs [13,20–22]. No LT-HSC activity was detected within the early regenerating HPC-2 population, even when transplanting high numbers. The HPC-2 population has been investigated previously at SS [13,21,53]; we confirm that during regeneration, it harbors no stem cells.

It has previously been reported that HSCs maintain their lineage bias identity when they are transplanted [2,4]. Our results suggest that, on a population level, regenerating HSCs have similar lineage potential and that the regeneration process does not select for or alter the composition of the HSC pool in that respect. The severe stress inflicted by transplantation does, however, reduce the magnitude of their reconstitution potential. We observed an inverse correlation between time after primary transplantation and reconstitution potential in a secondary host, in which HSCs isolated early after primary transplant showed lower reconstitution levels than those isolated late after primary transplant. One plausible key determinant for this functional difference is cell cycle, which was upregulated in early HSCs. The cell cycle is a major determinant for transcriptional heterogeneity linked to function in HSCs at SS, and our results confirm that this holds during regeneration as well [36]. Moreover, recent findings

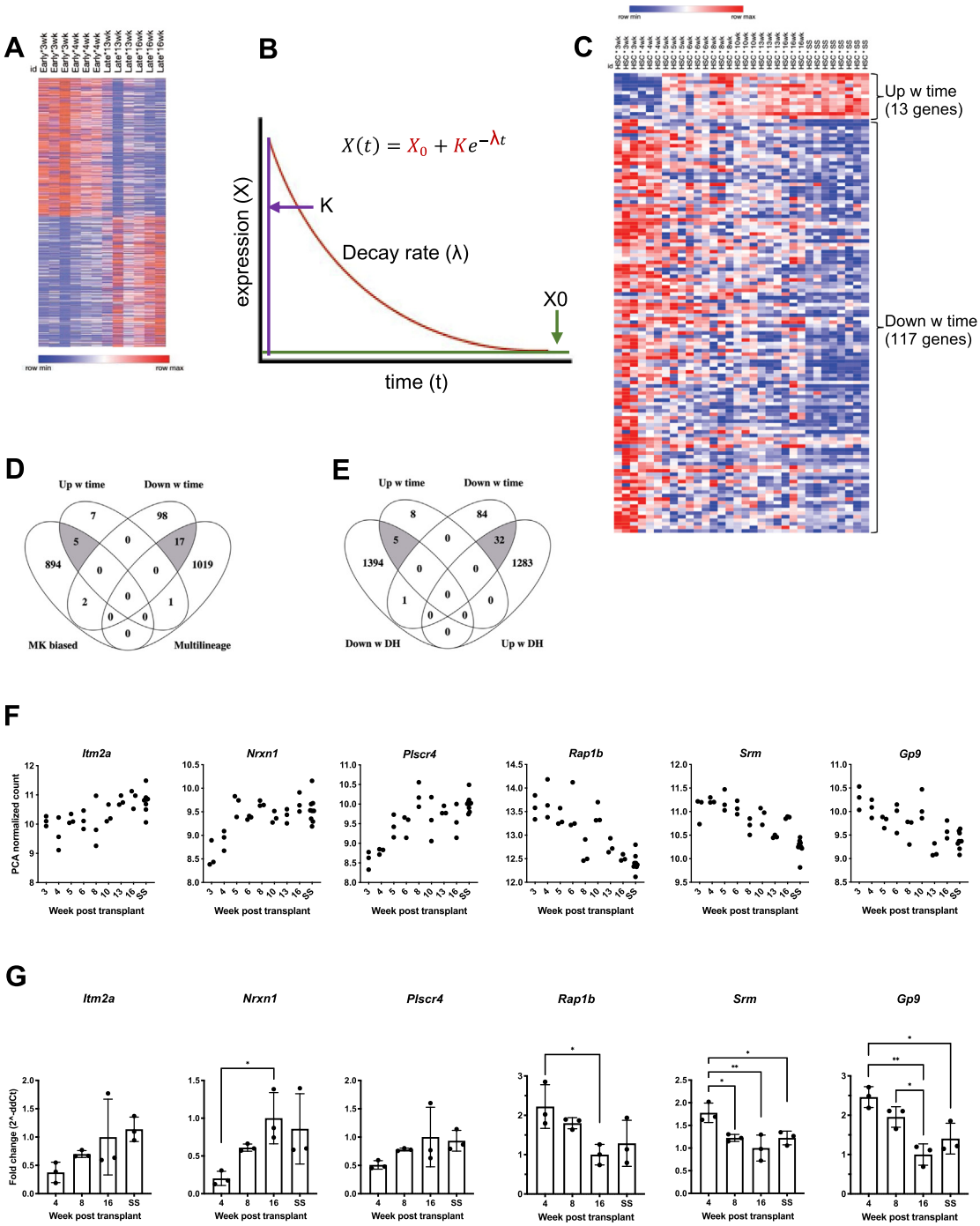

Figure 4 Model fit of regenerating HSC transcriptome. **(A)** Heat map of 1,060 DEG between early versus late HSCs. *Padj* < 0.1 and log2FC > 1.

(B) Mathematical model based on the assumption that the expression (x) of a given gene increases or decreases with a decay rate (λ) over time (t) after transplantation.

(C) Heat map of 13 genes with increased expression and 117 genes with decreased expression over time after transplantation.

(D) Overlap of genes in heat map **(C)** with gene list based on historical progeny output.

(E) Overlap of genes in heat map **(C)** with gene list based on DH.

(F) RNA sequencing expression of selected genes in heat map **(C)**.

(G) qPCR validation of genes in **(F)**. Data represented as mean ± SD. N = 3. Gene expression levels were normalized to the housekeeping gene *Hprt* and adjusted to 1 for the 16-week samples. Statistical significance was calculated using ordinary 1-way ANOVA in combination with Tukey's correction for multiple comparisons. Significance is indicated as *$Padj \leq 0.05$; **$Padj \leq 0.01$.

suggest that the main output of this increase in proliferation early after transplantation is the production of mature blood cells rather than a replenishment of the stem cell pool by self-renewal [15].

We aimed to identify genes with a gradual increase or decrease in expression as a response to transplantation that could be linked to the change in reconstitution capacity seen over time, thereby possibly acting as regulators of HSCs. Our approach was to integrate the HSC transcriptomes sampled at 8 different time points after transplantation into a decay rate model. This would cover all regenerative phases of HSCs and allow for a comprehensive analysis that a binary comparison of early versus late HSCs would not include.

Interestingly, not only did it reduce the number of genes significantly, but of the 130 genes identified with this approach, only 22 were overlapping with the 1,060 differentially expressed genes (DEG) in the early versus late DESeq2 analysis, highlighting the different outcomes of the 2 approaches. Most of the 130 genes were previously not attributed regulatory functions of HSCs. The significant and relevant overlaps with the data sets from Camargo and Moore [46,47], including genes with diverse biological functions, combined with our independent validation of selected genes by qPCR makes this data set a valuable source for further mining and exploration.

Conflict of Interest Disclosure

The authors do not have any conflicts of interest to declare in relation to this work.

Acknowledgments

This work was funded by Knut och Alice Wallenbergs Stiftelse. Additionally, the Swedish Research Council, Cancerfonden, and the Swedish Pediatric Cancer Society funded the study with grants to Dr. SK. This work was supported by Core-to-Core Program Advanced Research Networks "Integrative approach for normal and leukemic stem cells" from the Japan Society for the Promotion of Science of Japan. We thank Alexandra Rundberg-Nilsson for valuable input on the manuscript.

Author Contributions

AR, THMG, EM, MvdG, AS, TE, BN, KM, JL, and SK planned the study and designed the experiments. AR and THMG performed the majority of the experiments with assistance from EM, MvdG and AS. AR and THMG analyzed the majority of the experiments. AN and SS performed the bioinformatic analysis with assistance from AR. MP performed the RNA sequencing. AR, JL, and SK drafted the manuscript. All coauthors contributed to the final manuscript.

SUPPLEMENTARY MATERIALS

Supplementary material associated with this article can be found in the online version at https://doi.org/10.1016/j.exphem.2023.08.010.

REFERENCES

1. Benz C, Copley MR, Kent DG, et al. Hematopoietic stem cell subtypes expand differentially during development and display distinct lymphopoietic programs. Cell Stem Cell 2012;10:273–83.
2. Yu VWC, Yusuf RZ, Oki T, et al. Epigenetic memory underlies cell-autonomous heterogeneous behavior of hematopoietic stem cells. Cell 2016;167. 1310–1322.e17.
3. Cabezas-Wallscheid N, Buettner F, Sommerkamp P, et al. Vitamin A-retinoic acid signaling regulates hematopoietic stem cell dormancy. Cell 2017;169. 807–823.e19.
4. Carrelha J, Meng Y, Kettyle LM, et al. Hierarchically related lineage-restricted fates of multipotent haematopoietic stem cells. Nature 2018;554:106–11.
5. Ceredig R, Rolink AG, Brown G. Models of haematopoiesis: seeing the wood for the trees. Nat Rev Immunol 2009;9:293–300.
6. Zhang Y, Gao S, Xia J, Liu F. Hematopoietic hierarchy—an updated roadmap. Trends Cell Biol 2018;28:976–86.
7. Sun J, Ramos A, Chapman B, et al. Clonal dynamics of native haematopoiesis. Nature 2014;514:322–7.
8. Busch K, Klapproth K, Barile M, et al. Fundamental properties of unperturbed haematopoiesis from stem cells in vivo. Nature 2015;518:542–6.
9. Kiel MJ, Yilmaz OH, Iwashita T, Yilmaz OH, Terhorst C, Morrison SJ. SLAM family receptors distinguish hematopoietic stem and progenitor cells and reveal endothelial niches for stem cells. Cell 2005;121:1109–21.
10. Forsberg EC, Serwold T, Kogan S, Weissman IL, Passegué E. New evidence supporting megakaryocyte-erythrocyte potential of flk2/flt3+ multipotent hematopoietic progenitors. Cell 2006;126:415–26.
11. Venezia TA, Merchant AA, Ramos CA, et al. Molecular signatures of proliferation and quiescence in hematopoietic stem cells. PLoS Biol 2004;2:e301.
12. Wilson A, Laurenti E, Oser G, et al. Hematopoietic stem cells reversibly switch from dormancy to self-renewal during homeostasis and repair. Cell 2008;135:1118–29.
13. Pietras EM, Reynaud D, Kang YA, et al. Functionally distinct subsets of lineage-biased multipotent progenitors control blood production in normal and regenerative conditions. Cell Stem Cell 2015;17:35–46.
14. Randall TD, Weissman IL. Phenotypic and functional changes induced at the clonal level in hematopoietic stem cells after 5-fluorouracil treatment. Blood 1997;89:3596–606.
15. Dong F, Hao S, Zhang S, et al. Differentiation of transplanted haematopoietic stem cells tracked by single-cell transcriptomic analysis. Nat Cell Biol 2020;22:630–9.
16. Love MI, Huber W, Anders S. Moderated estimation of fold change and dispersion for RNA-seq data with DESeq2. Genome Biol 2014;15:550.
17. Ritchie ME, Phipson B, Wu D, et al. limma powers differential expression analyses for RNA-sequencing and microarray studies. Nucleic Acids Res 2015;43:e47.
18. Subramanian A, Tamayo P, Mootha VK, et al. Gene set enrichment analysis: a knowledge-based approach for interpreting genome-wide expression profiles. Proc Natl Acad Sci U S A 2005;102:15545–50.
19. Santaguida M, Schepers K, King B, et al. JunB protects against myeloid malignancies by limiting hematopoietic stem cell proliferation and differentiation without affecting self-renewal. Cancer Cell 2009;15:341–52.
20. Chapple RH, Tseng YJ, Hu T, et al. Lineage tracing of murine adult hematopoietic stem cells reveals active contribution to steady-state hematopoiesis. Blood Adv 2018;2:1220–8.
21. Säwen P, Eldeeb M, Erlandsson E, et al. Murine HSCs contribute actively to native hematopoiesis but with reduced differentiation capacity upon aging. Elife 2018;7:e41258.
22. Upadhaya S, Sawai CM, Papalexi E, et al. Kinetics of adult hematopoietic stem cell differentiation in vivo. J Exp Med 2018;215:2815–32.

23. Wilson A, Murphy MJ, Oskarsson T, et al. c-Myc controls the balance between hematopoietic stem cell self-renewal and differentiation. Genes Dev 2004;18:2747–63.
24. Chen C, Liu Y, Liu R, et al. TSC-mTOR maintains quiescence and function of hematopoietic stem cells by repressing mitochondrial biogenesis and reactive oxygen species. J Exp Med 2008;205:2397–408.
25. Laurenti E, Varnum-Finney B, Wilson A, et al. Hematopoietic stem cell function and survival depend on c-Myc and N-Myc activity. Cell Stem Cell 2008;3:611–24.
26. Wu F, Chen Z, Liu J, Hou Y. The Akt-mTOR network at the interface of hematopoietic stem cell homeostasis. Exp Hematol 2021;103:15–23.
27. Ito K, Carracedo A, Weiss D, et al. A PML-PPAR-delta pathway for fatty acid oxidation regulates hematopoietic stem cell maintenance. Nat Med 2012;18:1350–8.
28. Guo F, Zhang S, Grogg M, et al. Mouse gene targeting reveals an essential role of mTOR in hematopoietic stem cell engraftment and hematopoiesis. Haematologica 2013;98:1353–8.
29. Oburoglu L, Romano M, Taylor N, Kinet S. Metabolic regulation of hematopoietic stem cell commitment and erythroid differentiation. Curr Opin Hematol 2016;23:198–205.
30. Basu S, Broxmeyer HE, Hangoc G. Peroxisome proliferator-activated-γ coactivator-1α-mediated mitochondrial biogenesis is important for hematopoietic recovery in response to stress. Stem Cells Dev 2013;22:1678–92.
31. Yamashita M, Passegué E. TNF-alpha coordinates hematopoietic stem cell survival and myeloid regeneration. Cell Stem Cell 2019;25. 357−372.e7.
32. Essers MA, Offner S, Blanco-Bose WE, et al. IFNalpha activates dormant haematopoietic stem cells in vivo. Nature 2009;458:904–8.
33. Sato T, Onai N, Yoshihara H, Arai F, Suda T, Ohteki T. Interferon regulatory factor-2 protects quiescent hematopoietic stem cells from type I interferon-dependent exhaustion. Nat Med 2009;15:696–700.
34. Walter D, Lier A, Geiselhart A, et al. Exit from dormancy provokes DNA-damage-induced attrition in haematopoietic stem cells. Nature 2015;520:549–52.
35. Ivanova NB, Dimos JT, Schaniel C, Hackney JA, Moore KA, Lemischka IR. A stem cell molecular signature. Science 2002;298:601–4.
36. Lauridsen FKB, Jensen TL, Rapin N, et al. Differences in cell cycle status underlie transcriptional heterogeneity in the HSC compartment. Cell Rep 2018;24:766–80.
37. Min IM, Pietramaggiori G, Kim FS, Passegué E, Stevenson KE, Wagers AJ. The transcription factor EGR1 controls both the proliferation and localization of hematopoietic stem cells. Cell Stem Cell 2008;2:380–91.
38. Amrani YM, Gill J, Matevossian A, et al. The Paf oncogene is essential for hematopoietic stem cell function and development. J Exp Med 2011;208:1757–65.
39. Lee SC, Miller S, Hyland C, et al. Polycomb repressive complex 2 component Suz12 is required for hematopoietic stem cell function and lymphopoiesis. Blood 2015;126:167–75.
40. Lüscher-Firzlaff J, Chatain N, Kuo CC, et al. Hematopoietic stem and progenitor cell proliferation and differentiation requires the trithorax protein. Ash2l. Sci Rep. 2019;9:8262.
41. Grahn THM, Niroula A, Végvári Á, et al. S100A6 is a critical regulator of hematopoietic stem cells. Leukemia 2020;34:3323–37.
42. Sun S, Wang W, Latchman Y, Gao D, Aronow B, Reems JA. Expression of plasma membrane receptor genes during megakaryocyte development. Physiol Genomics 2013;45:217–27.
43. Savoia A, Kunishima S, De Rocco D, et al. Spectrum of the mutations in Bernard-Soulier syndrome. Hum Mutat 2014;35:1033–45.
44. Singh D, Upadhyay G, Sengupta A, et al. Cooperative stimulation of megakaryocytic differentiation by Gfi1b gene targets Kindlin3 and Talin1. PLoS One 2016;11:e0164506.
45. Jiang L, Wang X, Wang Y, Chen X. Quantitative proteomics reveals that miR-222 inhibits erythroid differentiation by targeting BLVRA and CRKL. Cell Biochem Funct 2018;36:95–105.
46. Rodriguez-Fraticelli AE, Weinreb C, Wang SW, et al. Single-cell lineage tracing unveils a role for TCF15 in haematopoiesis. Nature 2020;583:585–9.
47. Bernitz JM, Rapp K, Daniel MG, et al. Memory of divisional history directs the continuous process of primitive hematopoietic lineage commitment. Stem Cell Reports 2020;14:561–74.
48. Kodigepalli KM, Bowers K, Sharp A, Nanjundan M. Roles and regulation of phospholipid scramblases. FEBS Lett 2015;589:3–14.
49. Namkoong S, Lee KI, Lee JI, et al. The integral membrane protein ITM2A, a transcriptional target of PKA-CREB, regulates autophagic flux via interaction with the vacuolar ATPase. Autophagy 2015;11:756–68.
50. Rho SS, Kobayashi I, Oguri-Nakamura E, et al. Rap1b promotes Notch-signal-mediated hematopoietic stem cell development by enhancing integrin-mediated cell adhesion. Dev Cell 2019;49. 681−696.e6.
51. Stefanini L, Bergmeier W. RAP GTPases and platelet integrin signaling. Platelets 2019;30:41–7.
52. Forshell TP, Rimpi S, Nilsson JA. Chemoprevention of B-cell lymphomas by inhibition of the Myc target spermidine synthase. Cancer Prev Res (Phila) 2010;3:140–7.
53. Oguro H, Ding L, Morrison SJ. SLAM family markers resolve functionally distinct subpopulations of hematopoietic stem cells and multipotent progenitors. Cell Stem Cell 2013;13:102–16.